THE DRAG-BASED MODEL (DBM) with constant solar wind speed

Model Developer(s)

T. Žic, B. Vršnak
Hvar Observatory, Faculty of Geodesy, University of Zagreb

Model Description

The Drag-Based Model (DBM) tool provides predictions of the ICME travel and its arrival at arbitrary ecliptic-plane location or at already listed planets and satellites in ecliptic-plane orbits. Calculations are based on the assumption that the dominant force in the heliospheric dynamics of ICMEs is the magnetohydrodynamical equivalent of the aerodynamic drag (for details see Vršnak et al. [2013], and references therein). The background solar wind is based on the approximation that is approximately stationary and isotropic and its speed w is constant Vršnak and Žic [2007]. From these approximations follows that the drag-parameter γ is constant as well. Basically, for a given set of input parameters the model provides the ICME Sun-"target" transit time, the arrival time, and the impact speed Vršnak and Žic [2007].

The web-tool is divided into the basic and advanced form. The purpose of the basic form is to predict the radial heliocentric ICME propagation (position-time, $R(t)$, coupled with speed-position, $v(R)$, plots), arrival time and impact speed at selected "target" in the ecliptic plane. Additionally, the advanced form of DBM (with constant w and γ) calculates this output for the target in the heliosphere taking into account also the shape of ICME employing the so-called cone-geometry [see Apendix in Žic et al., 2015].

Model Input

The inputs of the basic form of the DBM (with constant w and γ) are CME take-off date and time; constant value of drag parameter, γ; constant value of solar wind speed, w; starting radial distance and speed of CME (R_0 and v_0, respectively); the selected (or manually entered) target distance and from these values the DBM calculates the date and time of CME arrival, its transit time and impact speed on preselected target, accompanied with heliocentric $v(R)$ and $R(t)$ plots. Additionally, the advanced form requires the CME angular half-width, ω, and source region central meridian distance, φ, from which the DBM using cone-geometry estimates ICME impact parameters, kinematic plots and produce the time dependent cone-geometry animated plot.

Model Output

The principal output is composed of the predicted ICME kinematics, ICME arrival and impact parameters (*e.g.* impact speed) for arbitrary entered location on the ecliptic plane. The DBM tool is basically focused on the ICME arrival at Earth position.

References and relevant publications

- Vršnak, 2001
- Vršnak and Žic, 2007
- Vršnak et al., 2010
- Vršnak et al., 2013
- Žic et al., 2015

Relevant links

- Development site: http://www.geof.unizg.hr/~tzic/dbm.html.
- Official site of the previous version: http://oh.geof.unizg.hr/DBM/dbm.php

Developer Contact(s)

Tomislav Žic (tzic@geof.hr)

A Detailed description

One of the central issues of the COMESEP project is forecasting of the ICME arrival to the Earth or any other point in the heliosphere. The main tool foreseen to provide predictions of the ICME arrival to the "target" is the so-called Drag-Based Model (DBM). The basic form of the model was formulated by Vršnak and Žic [2007] and was advanced and adjusted for the COMESEP purposes by Vršnak et al. [2013]. The model is based on the assumption that beyond certain heliocentric distance the ICME propagation is governed solely by its interaction with the ambient solar wind, *i.e.*, that acceleration/deceleration of the ICME can be expressed in terms of the magnetohydrodynamical (MHD) analogue of the aerodynamic drag (for details see Cargill et al., 1996).

A.1 Basic form

In DBM, the ICME propagation is determined by the equation of motion which reads

$$a = -\gamma\,(v-w)\,|v–w| \tag{1}$$

where a and v are the instantaneous ICME acceleration and speed, w is the instantaneous ambient solar-wind speed, and γ is the so-called drag parameter, or drag efficiency. Note that all quantities in Equation (1) are time/space dependent. Equation (1) reflects the most basic characteristics of the ICME heliospheric propagation: ICMEs that are faster than the ambient solar wind are decelerated, whereas those slower than the solar wind are accelerated by the ambient flow (cf., Gopalswamy et al., 2000).

Bearing in mind $a = \partial^2 R/\partial t^2$ and $v = \partial R/\partial t$, Equation (1) provides kinematics of the ICME apex, $R(t)$, $v(t)$, $v(R)$, for given initial conditions, $t = 0$, $R = R_i$, $v = v_i$, and the asymptotic values $\gamma(R \to \infty) = \gamma_\infty$ and $w(R \to \infty) = w_\infty$. The drag parameter γ defines the velocity change-rate, *i.e.*, shows for how much the ICME speed changes over the unit-distance. It can be expressed as:

$$\gamma = c_d \frac{A\,\rho_{\rm SW}}{M} \tag{2}$$

where c_d is a dimensionless drag coefficient, usually being on the order of 1 (for details see Cargill, 2004), A and M are the ICME cross section and mass, respectively, whereas $\rho_{\rm SW}$ is the density of the ambient solar wind. The unit for γ in M.K.S. system is m^{-1}; however, for practical reasons, in the following we will use the dimensionless abbreviation Γ defined by $\gamma = \Gamma \times 10^{-7}\,\mathrm{km}^{-1}$. Note that at sufficiently large distances (say, $R > 20\,r_{\rm Sun}$, where $r_{\rm Sun}$ is the solar radius) the following approximations are valid: $A \propto R^2$, $\rho_{\rm SW} \propto 1/R^2$, $M = const.$, and $c_d = const.$ (for details, see Cargill, 2004), implying $\gamma = const. = \gamma_\infty$. Finally, note that in the following we will denote the asymptotic values w_∞ and γ_∞ simply as w and γ. The parameter γ can be expressed alternatively also as:

$$\gamma = c_d \frac{A\,\rho_{\rm SW}}{V_{\rm ICME}\,\rho_{\rm ICME}} \approx c_d \frac{1}{L}\frac{\rho_{\rm SW}}{\rho_{\rm ICME}}, \tag{3}$$

where $V_{\rm ICME}$, L, and $\rho_{\rm ICME}$ are the ICME volume, thickness, and density, respectively. Equation (3) shows that massive ICMEs that are much denser than the ambient solar wind are affected by the drag much less than light ICMEs.

For the solar wind density we employ the empirical model by Leblanc et al. [1998], which asymptotically behaves as $\rho \sim 1/R^2$. Assuming the isotropic solar wind, *i.e.*, $\rho w R^2 = const.$, this defines the solar-wind speed, with the asymptotic value $w_\infty = const.$

A.2 DBM with cone geometry

The DBM formulation presented above does not take into account the ICME shape, *i.e.*, it provides the calculation of the kinematics only for the ICME apex. In the advanced form, the model takes into account also the shape of ICME. In the following, we employ the so-called cone-geometry; in Figure 1 three standard cone options are depicted (see Schwenn et al., 2005 and references therein).

In the option shown in Figure 1a the ICME leading edge is a circular arc concentric with the solar surface, *i.e.*, all elements of the ICME front have the same heliocentric distance. Under such conditions, the basic form of DBM can be applied for any angle α within the cone of angular half-width ω. In the second option, shown in Figure 1b, the leading edge is considered to be a semi-circle, spanning over the ICME full angular width, 2ω. The option drawn in Figure 1c, represents a self-similarly expanding ICME, whose leading edge is a circular arc that tangentially connects to the ICME legs. Note that this option

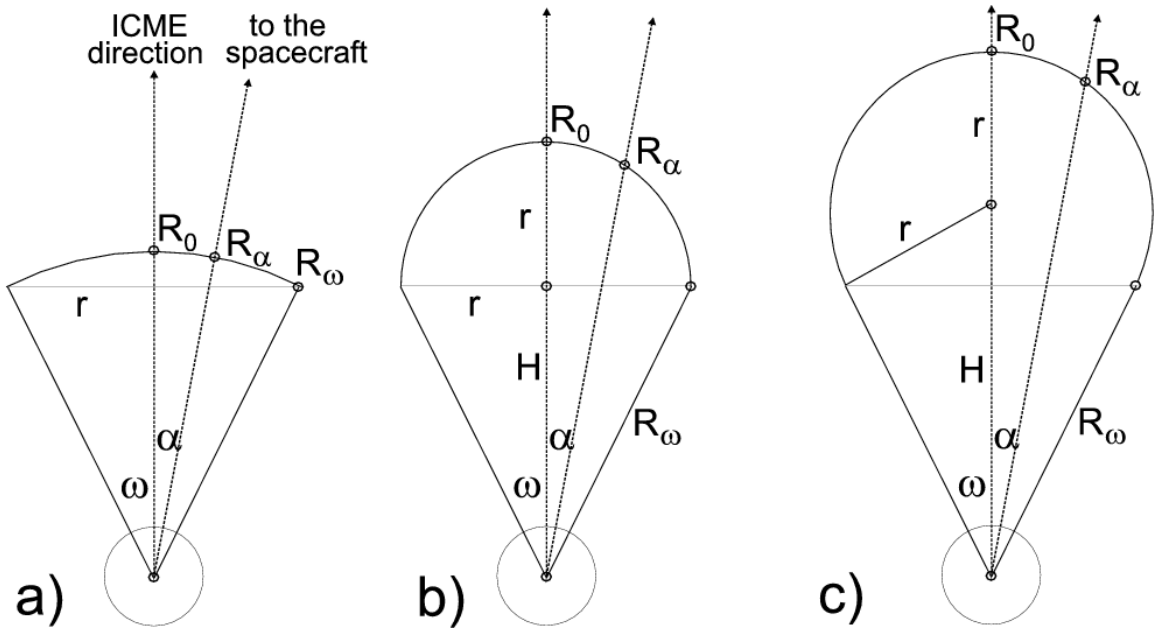

Figure 1: Three options of the ICME cone-geometry.

is analogous to the self-similarly expanding ICME model introduced by Lugaz et al. [2010] and advanced by Davies et al. [2012] and Möstl and Davies [2012]. Thus, hereinafter we will not consider this shape; we just refer to the three mentioned references. Instead we focus on the option shown in Figure 1b.

Considering relationships between various geometrical parameters marked in Figure 1b, we find for an ICME of the angular half-width ω:

$$\begin{aligned} R_0 &= H + r, \\ r &= H\,\tan\omega, \\ R_\alpha &= H\cos\alpha + \sqrt{r^2 - H^2\sin^2\alpha}, \end{aligned}$$

from which we find the relationship between the heliocentric distance of the ICME apex, R_0, and the element located at the angle α, R_α:

$$R_\alpha = R_0 \frac{\cos\alpha + \sqrt{\tan^2\omega - \sin^2\alpha}}{1 + \tan\omega}. \tag{4}$$

Taking a time derivative of Equation (4) we also find analogous relationship for the speed:

$$v_\alpha = v_0 \frac{\cos\alpha + \sqrt{\tan^2\omega - \sin^2\alpha}}{1 + \tan\omega}, \tag{5}$$

where v_0 is the ICME apex speed, and v_α is the speed of the leading-edge element at the angle α.

In Figure 2 the distance ratio R_α/R_0 is visualized by showing it as a function of the angle α for various ICME half-widths ω. The same graph applies also for the speed ratio v_α/v_0. Note that the value of α is limited, $0 \le \alpha \le \omega$, where $\alpha = 0$ corresponds to the apex direction and $\alpha = \omega$ corresponds to the lateral edge of the ICME. Inspecting the graph, one finds that the ratio decreases non-linearly with increasing α for any half-width ω. The minimal value of the ratio R_α/R_0 increases with the increasing half-width ω, until $\omega = 45$ deg, where the lowest value, $R_\alpha/R_0 = 0.707$, is attained. For half-widths $\omega > 45$ deg, the minimal value of R_α/R_0 increases again and at $\omega = 90$ deg, representing the ICME of the form of semi-circle, it becomes $R_\alpha/R_0 = 1$ for any value of α. The envelope connecting the minimal values of the ratio R_α/R_0 is drawn in Figure 2 by the red dashed line.

After the geometrical relationships have been established, there are two possibilities for the DBM application, in both cases assuming that the ICME angular half-width ω does not change:

i) The straightforward one is to follow the DBM kinematics of the ICME apex starting from initial apex heliocentric distance $R_0(t = 0) \approx R_{0i}$ and speed, $v_0(t = 0) \approx v_{0i}$ and then,

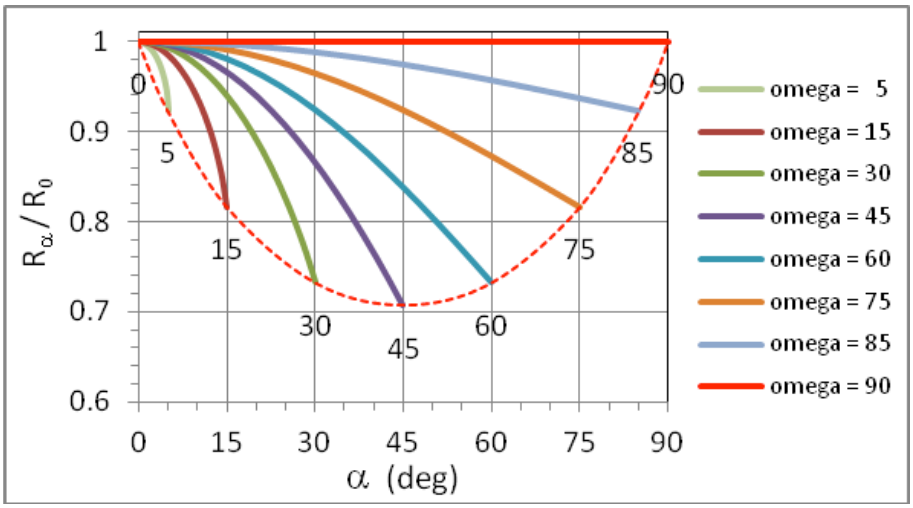

Figure 2: Ratio of the heliocentric distance of the ICME leading-edge segment located at the angle α and the distance of the apex, presented as a function of α for various cone half-widths ω.

assuming that the overall ICME shape remains unchanged, to apply Equations (4) and for each calculation-step in order to find the instantaneous distance $R_\alpha(t)$ and speed v_α of the ICME element moving along the angle α;

ii) A complementary, and probably more realistic alternative, is to find first the initial distance $R_{\alpha i}$ and speed $v_{\alpha i}$ of the ICME element at the angle α by substituting R_{0i} and v_{0i} into Equations (4) and (5), and then, to follow the DBM kinematics of this element independently.

Note that in the option *ii*) the initial circularly-shaped ICME front deforms in time, since the flanks move slower (Equation (5)), thus in fast ICMEs the drag-deceleration of flanks is weaker, whereas flank acceleration in slow events is stronger. Consequently, the variation of speed along the ICME front decreases and the front gradually flattens, asymptotically transforming into the shape depicted in Figure 1a.

In Figure 3 we compare the ICME kinematics simulated by the two DBM alternatives mentioned above. The displayed results are calculated for the ICME of half-width of $\omega = 30\,\mathrm{deg}$, applying $\Gamma = 0.2$ and the solar wind speed of $w = 400\,\mathrm{km/s}$, and taking as input $R_{0i} = 20\,r_{\mathrm{Sun}}$ and $v_{0i} = 1000\,\mathrm{km/s}$. Inspecting the graphs, one finds that the difference between kinematics of different ICME segments is larger for the DBM/alternative-*i* (top). In the DBM/alternative-*ii* the speeds of all segments converge, reflecting the fact that the ICME front changes shape. The 1 AU transit time increases towards the ICME edge (check the intersect of the kinematical curves and the upper border of the $R(t)$ graphs, set at $R = 1\,\mathrm{AU}$), the increase being larger for the DBM/alternative-*i*. For the chosen parameters, the flank transit time calculated by the DBM/alternative-*i* is for $\approx 30\,\mathrm{h}$ longer than for the apex, whereas in the case of the DBM/ alternative-*ii* the difference is around 10 h.

References

P. J. Cargill. On the Aerodynamic Drag Force Acting on Interplanetary Coronal Mass Ejections. *Solar Phys.*, 221:135–149, May 2004. doi: 10.1023/B:SOLA.0000033366.10725.a2.

P. J. Cargill, J. Chen, D. S. Spicer, and S. T. Zalesak. Magnetohydrodynamic simulations of the motion of magnetic flux tubes through a magnetized plasma. *J. Geophys. Res.*, 101:4855–4870, March 1996. doi: 10.1029/95JA03769.

J. A. Davies, R. A. Harrison, C. H. Perry, C. Möstl, N. Lugaz, T. Rollett, C. J. Davis, S. R. Crothers, M. Temmer, C. J. Eyles, and N. P. Savani. A Self-similar Expansion Model for Use in Solar Wind Transient Propagation Studies. *Astrophys. J.*, 750:23, May 2012. doi: 10.1088/0004-637X/750/1/23.

N. Gopalswamy, A. Lara, R. P. Lepping, M. L. Kaiser, D. Berdichevsky, and O. C. St. Cyr. Interplanetary acceleration of coronal mass ejections. *Geophys. Res. Lett.*, 27:145–148, 2000. doi: 10.1029/1999GL003639. URL http://dx.doi.org/10.1029/1999GL003639.

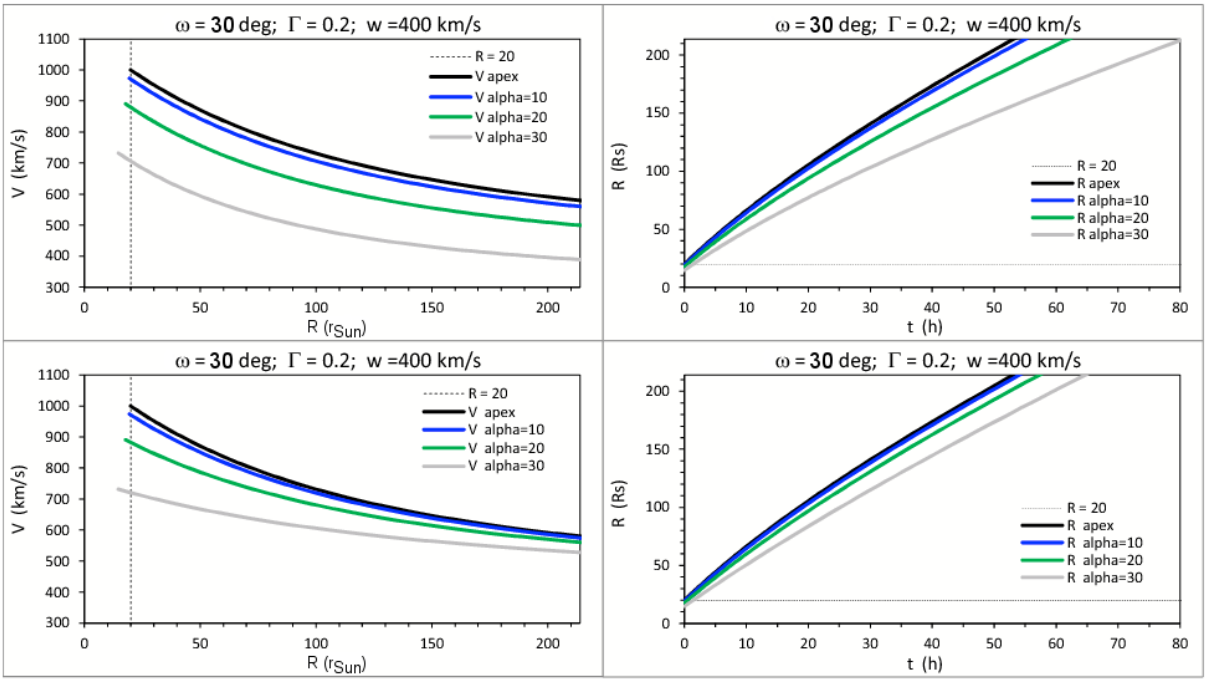

Figure 3: Speed of a given ICME segment versus the heliospheric distance (left) and the distance versus time for an ICME of the width of $\omega = 30\,\mathrm{deg}$, calculated using DBM/alternative-*i* (top) and DBM/alternative-*ii* (bottom), for various values of α. The distance of $R = 20\,r_{\mathrm{Sun}}$ is marked by the gray-dashed line.

Y. Leblanc, G. A. Dulk, and J.-L. Bougeret. Tracing the Electron Density from the Corona to 1 au. *Solar Phys.*, 183:165–180, 1998. ISSN 0038-0938. URL http://dx.doi.org/10.1023/A:1005049730506. 10.1023/A:1005049730506.

N. Lugaz, J. N. Hernandez-Charpak, I. I. Roussev, C. J. Davis, A. Vourlidas, and J. A. Davies. Determining the Azimuthal Properties of Coronal Mass Ejections from Multi-Spacecraft Remote-Sensing Observations with STEREO SECCHI. *Astrophys. J.*, 715:493–499, May 2010. doi: 10.1088/0004-637X/715/1/493.

C. Möstl and J. A. Davies. Speeds and Arrival Times of Solar Transients Approximated by Self-similar Expanding Circular Fronts. *Solar Phys.*, page 77, April 2012. doi: 10.1007/s11207-012-9978-8.

R. Schwenn, A. dal Lago, E. Huttunen, and W. D. Gonzalez. The association of coronal mass ejections with their effects near the Earth. *Ann. Geophys.*, 23:1033–1059, March 2005. doi: 10.5194/angeo-23-1033-2005.

B. Vršnak. Deceleration of Coronal Mass Ejections. *Solar Phys.*, 202:173–189, August 2001.

B. Vršnak and T. Žic. Transit times of interplanetary coronal mass ejections and the solar wind speed. *Astron. Astrophys.*, 472:937–943, September 2007. doi: 10.1051/0004-6361:20077499. URL http://dx.doi.org/10.1051/0004-6361:20077499.

B. Vršnak, T. Žic, T. V. Falkenberg, C. Möstl, S. Vennerstrom, and D. Vrbanec. The role of aerodynamic drag in propagation of interplanetary coronal mass ejections. *Astron. Astrophys.*, 512:A43, March 2010. doi: 10.1051/0004-6361/200913482. URL http://dx.doi.org/10.1051/0004-6361/200913482.

B. Vršnak, T. Žic, D. Vrbanec, M. Temmer, T. Rollett, C. Möstl, A. Veronig, J. Čalogović, M. Dumbović, S. Lulić, Y.-J. Moon, and A. Shanmugaraju. Propagation of Interplanetary Coronal Mass Ejections: The Drag-Based Model. *Solar Phys.*, 285:295–315, July 2013. doi: 10.1007/s11207-012-0035-4.

T. Žic, B. Vršnak, and M. Temmer. Heliospheric Propagation of Coronal Mass Ejections: Drag-Based Model Fitting. *Astrophys. J. Supp.*, 2015. submitted.